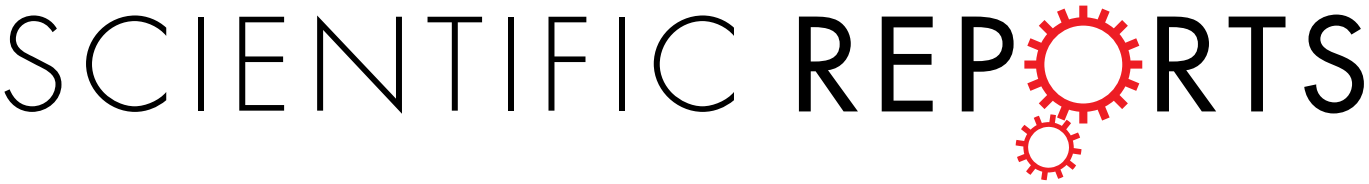

OPEN

Colloidal Organometal Halide Perovskite ($MAPbBr_xI_{3-x}$, $0 \leq x \leq 3$) Quantum Dots: Controllable Synthesis and Tunable Photoluminescence

Received: 02 September 2016
Accepted: 05 October 2016
Published: 24 October 2016

Ying Zhao[1], Xiangxing Xu[2] & Xiaozeng You[1]

Organic-inorganic perovskite materials, typically methylammonium lead trihalide ($MAPbX_3$: MA = methylammonium; X = Br, I), are recently attract enormous attention for their distinguished photo-electronic properties. The control of morphology, composition and dispersability of $MAPbX_3$ perovskite nanocrystals is crucial for the property tailoring and still a major challenge. Here we report the synthesis of colloidal $MAPbBr_xI_{3-x}$($0 \leq x \leq 3$) nanocrystals at room temperature by using alkyl carboxylate as capping ligands. These nanocrystals exhibit continuously tunable UV-vis absorption and photoluminescence (PL) across the visible spectrum, which is attributed to the quantum confinement effect with certain stoichiometry. Their unique exciton recombination dynamics was investigated and discussed.

Lead halide based perovskites have become famous semiconductor materials for their industrial prospect in solar cells. Up to date, the efficiency of perovskite solar cells has unceasingly boosted up to 22.1%[1–9]. The application potentials of perovskites in light emitting devices[10–17] and lasers[18,19] were also demonstrated. In nanometer scale, the huge specific surface area and thus the abundant interface or surface states of the perovskites exhibit prominent effects on the electronic and photoelectronic properties. Therefore, the challenge emerges for chemists of nano-science and -technology to develop synthesis methods to achieve size-controllable perovskite nanocrystals. In the most recent year, colloidal cesium lead halide perovskites nanocrystals and nanowires were successfully synthesized. Kovalenko *et al.* reported the synthesis of highly luminescent perovskite $CsPbX_3$(X = Cl, Br, I) of 4–15 nm, with the photoluminescence tuned within 410−700 nm[20,21]. Yang *et al.* developed a solution synthesis of single-crystalline $CsPbX_3$(X = Cl, Br, I) nanowires[22]. Prato *et al.* further found that the composition of perovskite nanocrystals can be feasibly tuned by post-synthesis halide anion exchange[23]. Despite the success for the all-inorganic cesium lead halide perovskite colloidal nanocrystals, the synthesis methods of colloidal organometal halide perovskite nanocrystals are comparably less developed. Although there are numerous literatures on preparing organic-inorganic perovskite micro/nanocrystals, most of them are synthesized or grow on substrates. For examples, the synthesis of $MAPbI_3$ nanoplates and nanowires on substrates were demonstrated by Jin[24], Horvath[25], Grätzel and Park *et al.*[26]. We reported the synthesis of $MAPbI_3$ crystals on porous TiO_2 substrate with the size controllable within 40–700 nm[27]. The substrates served as a scaffold for the precursors were used to control the perovskite growth kinetics[27–31]. However, the substrates prevented from scale up the products and the generality for different substrates is limited.

Recently, advances have been made in synthesis of $MAPbX_3$(X = Br, I, Cl) nanocrystals in solution without a substrate[32–36]. All these reported methods use organic ammonium cation with a long alkyl chain, such as the octylammonium bromide ($CH_3(CH_2)_7NH_3Br$) or octadecylammonium bromide ($CH_3(CH_2)_{17}NH_3Br$). The ammonium cation serves as the surface capping ligands of the nanocrystals, limiting the crystal growth in one, two or three dimensions. In this article, we use a different surface modulation strategy by applying alkyl

[1]State Key Laboratory of Coordination Chemistry, Collaborative Innovation Center of Advanced Microstructures, School of Chemistry and Chemical Engineering, Nanjing University, Nanjing 210093, PR China. [2]School of Chemistry and Materials Science, Nanjing Normal University, Nanjing 210023, PR China. Correspondence and requests for materials should be addressed to X.X. (email: xuxx@njnu.edu.cn) or X.Y. (email: youxz@nju.edu.cn)

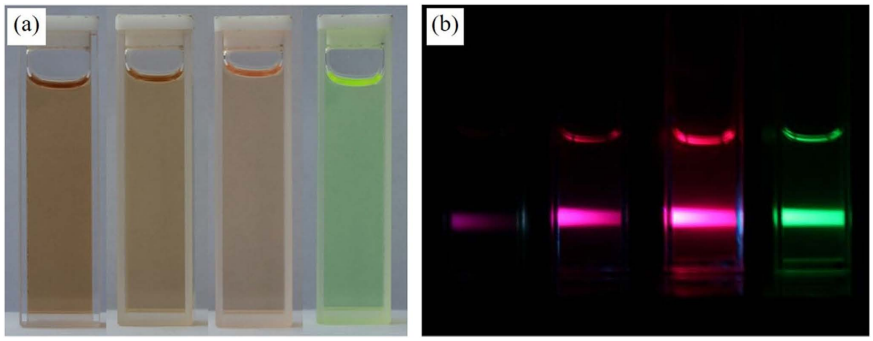

Figure 1. (**a**) Images of typical as synthesized $MAPbBr_xI_{3-x}(0 \leq x \leq 3)$ colloidal nanocrystals in solution under the day light and (**b**) images under the ultraviolet excitation (365 nm). From left to right: sample P-I-5, P-I3Br2-5, P-I1Br1-5 and P-Br-5.

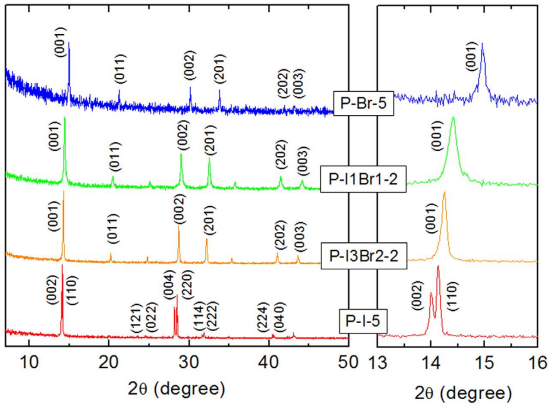

Figure 2. The XRD patterns of some typical as synthesized $MAPbBr_xI_{3-x}(0 \leq x \leq 3)$ nanocrystals: sample P-I-5, P-I3Br2-2, P-I1Br1-2 and P-Br-5.

carboxylate, the lead oleate ($Pb(CH_3(CH_2)_7CH=CH(CH_2)_7COO)_2$, abbreviated as $Pb(OA)_2$), as both the lead resource and capping ligands. The as synthesized $MAPbBr_xI_{3-x}(0 \leq x \leq 3)$ nanocrystals exhibit continuously tunable UV-vis absorption and photoluminescence (PL) spectra across the visible realm, which is attributed to the size related quantum confinement effect with a fixed stoichiometry of the halide composition.

Results and Discussion

The reaction solution contains two solvents, the cyclohexane and the isopropanol. The $Pb(OA)_2$ is soluble in the former, and the MAI or MABr (or the mixture) is soluble in the later. When these two solutions are mixed at room temperature, $MAPbBr_xI_{3-x}(0 \leq x \leq 3)$ forms immediately which can be easily identified by the color change and the photoluminescence under a portable 365 nm ultraviolet lamp (Fig. 1).

The XRD spectra of the typical products are shown in Fig. 2 (and Figures S1–S4 in Supporting Information). For the samples P-I-2/3/4/5, strong split peaks at 14.0° and 14.1° that respectively corresponding to (002) and (110) crystal plane and the split peaks of the (004) and (220) peaks can be clearly identified. This split feature verified that the as prepared $MAPbI_3$ are tetragonal perovskite phase (space group *I4/mcm*)[37–41]. While for the rest of the samples containing Br^-, no split can be identified at (001) or (002) peaks, indicating they are cubic phased perovskite (space group *Pm-3m*). The perovskite phases via the regulation of I^- and Br^- are generally observed by various researchers[38–41]. For all the samples no impurity of MAI or $Pb(OA)_2$ is found. This may due to the fast reaction rate and excess amount of MAI to consume the $Pb(OA)_2$. Also none of the other known and related MA_nPbI_m (n, m = 2,4, 3,5, 4,6) phases are observed[41].

For all the samples of $MAPbBr_xI_{3-x}(0 \leq x \leq 3)$ nanocrystals, the typical FTIR vibration modes of organolead halide perovskites are distinctly presented (Figure S5). The 3300–3000 cm^{-1} broad strong peak is assigned to N-H stretching; the 2950–2820 cm^{-1} peaks are assigned to symmetric and asymmetric stretching vibrations of CH_2 and CH_3[36,42–45]; the peak at 1730–1630 cm^{-1} corresponds to the COO^- modes and the peak at 1440–1360 cm^{-1} is assigned to the C-H bending[44]. The symmetric O-H stretch and antisymmetric O-H stretch of H_2O were not found in 3600–3800 cm^{-1} from Figure S5. Thus, no adsorbed H_2O was detected, suggesting its good temporary stability in ambient air condition. The good dispersability of the perovskites in cyclohexane also suggests that the surface of $MAPbBr_xI_{3-x}(0 \leq x \leq 3)$ nanocrystals is coordinated by oleate ligand, like typical oleate or alkylamines modified colloidal nanocrystals. The schematic illustration of a perovskite nanocrystal stabilized by oleate as surface ligands is shown in Fig. 3(a). Figure 3(b,c) are typical TEM and HRTEM images of perovskite nanocrystals

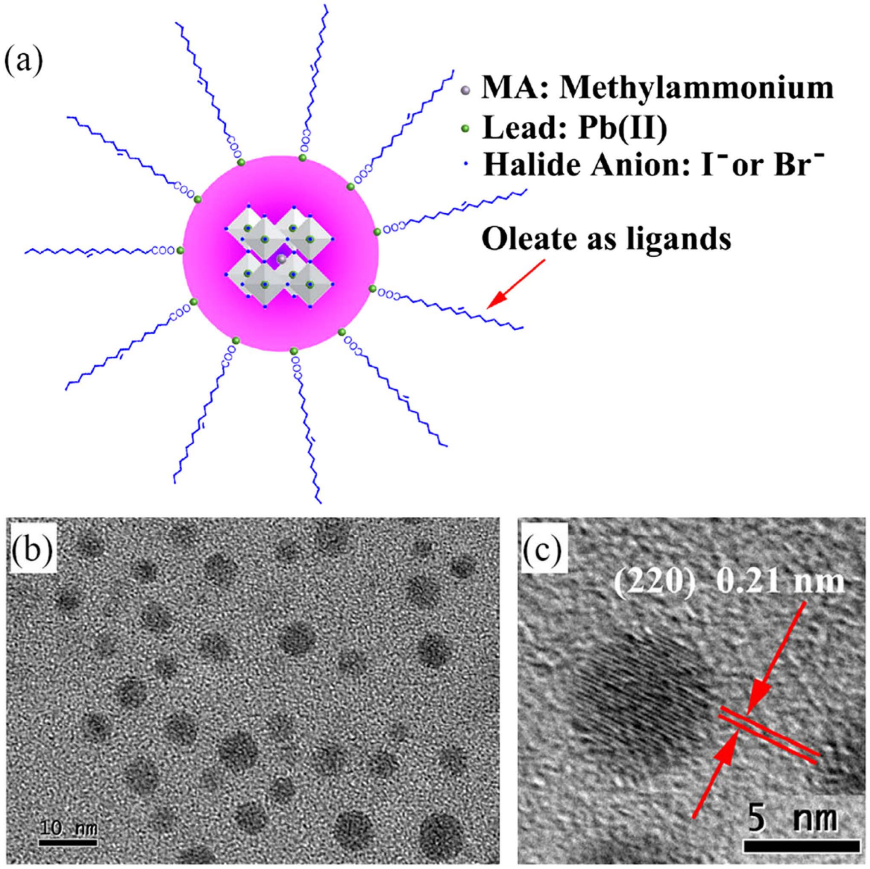

Figure 3. (**a**) Schematic illustration of a perovskite nanocrystals stabilized by oleate as surface ligands, (**b**) A typical TEM image and (**c**) HRTEM image of perovskite nanocrystals of sample P-Br-5.

of sample P-Br-5, respectively. It indicates that these nanocrystals are well dispersed and the measured crystal lattice matches well with the that of the $MAPbBr_3$[32,36]. Else TEM images of colloidal perovskite nanocrystals of $MAPbBr_xI_{3-x}(0 \leq x \leq 3)$ can be found in Figures S6–S8.

The SEM measurement indicates that with the decrement of MA:Pb from 5:1 to 2:1, the size of all the as synthesized $MAPbBr_xI_{3-x}(0 \leq x \leq 3)$ nanoparticles increases to ~300 nm (Fig. 4). This trend may find its origin in the nucleation and growth mechanism. Take the nucleation and growth of $MAPbI_3$ as an example, the reaction in the solution is as follows:

$$3MAI + Pb(OA)_2 \rightarrow MAPbI_3(colloidal) + 2OA^{2-} + 2MA^{+} \quad (1)$$

The alkyl carboxylate, lead oleate $Pb(OA)_2$, acts as not only as the lead resource to react with MAI, but also as the capping ligands. In addition, the reaction rate is higher with the higher MAI concentration. The faster the nucleation bursts, the more completely $Pb(OA)_2$ consumed in solution in a short time, leading to smaller $MAPbI_3$ nanocrystals. While in relatively lower MAI concentration, the nucleation rate is slower and the perovskite growth is dominated following the nucleation, resulting bigger $MAPbI_3$ nanocrystals. Obviously, it shows significance for all these perovskite materials.

The UV-vis absorption spectra and corresponding PL spectra of four sets of samples (P-I-2/3/4/5, P-I3Br2–2/3/4/5, P-I1Br1-2/3/4/5, P-Br-2/3/4/5) are shown in Fig. 5. The band edge absorption peak locates at 764 nm for big $MAPbI_3$ nanocrystals (P-I-2, ~300 nm by SEM). It undergoes a blue shift to 735 nm for smaller $MAPbI_3$ nanocrystals (P-I-5, ~5 nm by TEM). Accordingly, the photoluminescence (PL) peak shifts from 767 nm to 747 nm with the size decreasing. The synthesized $MAPbBr_3$ and $MAPbBr_xI_{3-x}(0 \leq x \leq 3)$ nanocrystals also show similar UV-vis absorption and PL spectra dependent on the size. This size related monotonic blue shift of both spectra can be induced by the intrinsic quantum confinement effect, for the small crystal size is comparable to the Bohr diameter of $MAPbBr_xI_{3-x}(0 \leq x \leq 3)$[46–50]. There remains only one concern, that since the spectra of P-I3Br2-2/3/4/5 and P-I1Br1-2/3/4/5 are over lapped, it is doubtful if the spectrum shift is caused by the component deviation. By comparing the XRD peaks of P-I3Br2-2/3/4/5 and P-I1Br1-2/3/4/5, this possibility is excluded. As shown in Fig. 6, the (002) and (201) peaks of each set are separated from each other, while almost fixed for a same set. It suggests that the perovskites of the same sets have the same crystal parameter, thus have the same component. Also, the widening of the XRD peaks indicates the size of nanocrystals decreases (Figures S1–S3). These features further support the intrinsic quantum confinement effect for the observed spectra shift.

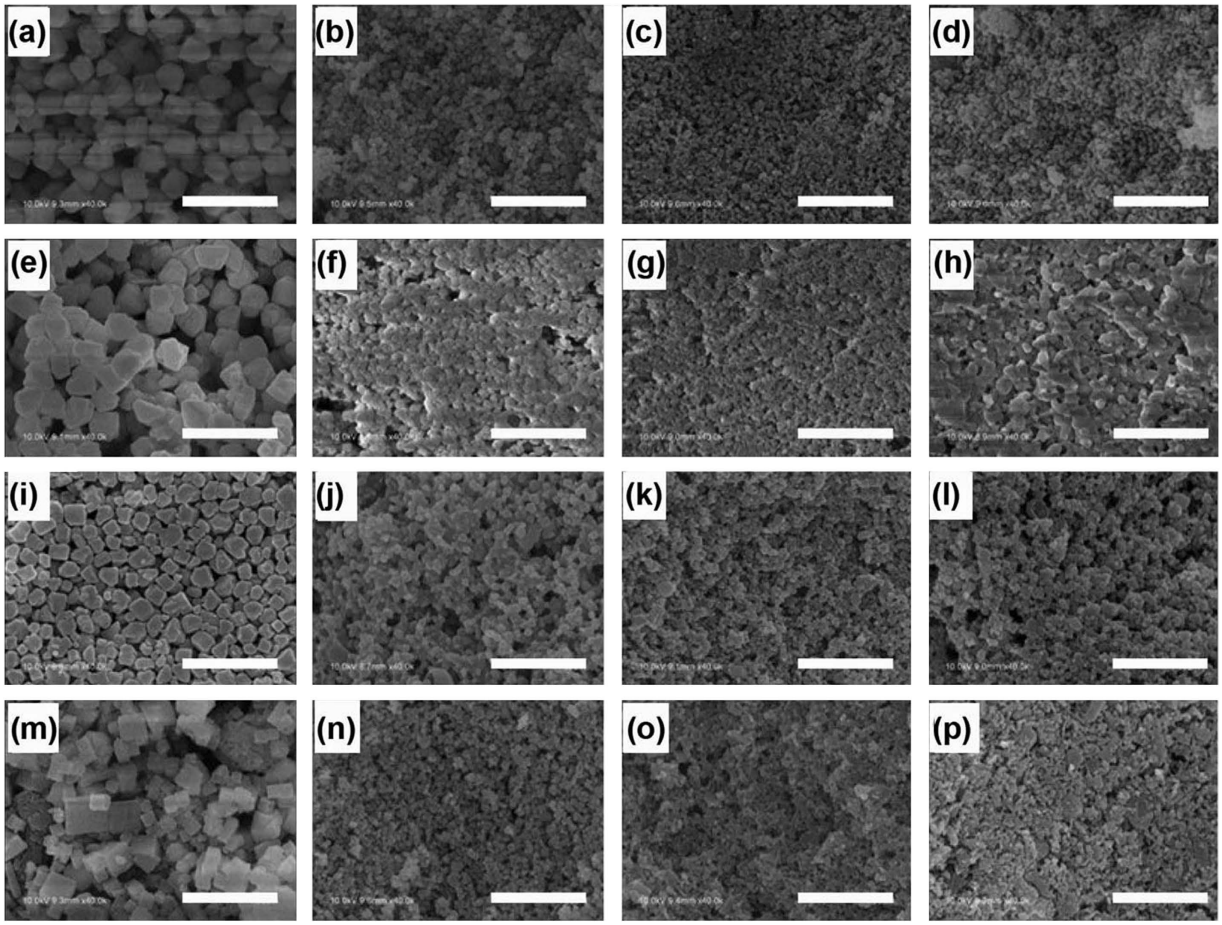

Figure 4. SEM images of four sets of samples (**a**–**d**) P-I-2/3/4/5 from left to right respectively, and the same for (**e**–**h**) P-I3Br2-2/3/4/5, (**i**–**l**) P-I1Br1-2/3/4/5, and (**m**–**p**) P-Br-2/3/4/5 (Scale bar: 1 μm).

The PL lifetimes of $MAPbBr_xI_{3-x}(0 \leq x \leq 3)$ were measured (Figures S9–11) to get insight into the exciton recombination dynamics. These PL decays can be well fitted by the bi-exponential function (Figure S12):

$$I(t) = A_1 \exp[-(t - t_0)/\tau_1] + A_2 \exp[-(t - t_0)/\tau_2] \quad (2)$$

where τ_1 and τ_2 are the fitted decay lifetimes; A_1 and A_2 are the weighting parameters. The average lifetime τ_{ave} is calculated by equation (3):

$$\tau_{ave} = (A_1\tau_1^2 + A_2\tau_2^2)/(A_1\tau_1 + A_2\tau_2) \quad (3)$$

The results are shown in Table 1. It suggests two dynamics, a fast decay (τ_1) and a longer-lived component (τ_2). With the decreasing size of the nanocrystal or the blue shift of the PL peak, the τ_{ave} increases for samples of P-I-2/3/4/5, P-I1Br1-2/3/4/5 and P-Br-2/3/4/5. For sample P-I-2, it has a very short lifetime τ_{ave} of 3.0 ns. The lifetime of the sample P-I-5 is incredibly prolonged to 166.2 ns. This lifetime range covers the ever reported lifetimes of tetragonal $MAPbI_3$ in the form of nanowire, nanorod, film or bulk (Table 2). A very short lifetime of P-I-2 indicates that there exist high effective nonradiative recombination channels in the material[50–52]. It is proposed to be chemical or structural defects in the $MAPbI_3$ nanocrystals. The long lifetime of the sample P-I-5 is unexpected, because it has a big specific surface area which may induce vast surface states. Possibly it suggests that the surface of $MAPbI_3$ nanocrystals is well passivated by the oleate ligands[53–55]. It was noticed that from P-I-2 to P-I-5, both τ_1 and τ_2 increase drastically. The fast decay τ_1 of P-I-5 is 25.5 ns, a value much bigger than the slow decay τ_2 of P-I-2 4.8 ns. The mechanisms how the τ_1 and τ_2 are separately or cohesively tuned are presently unclear. However, it is not likely to originate from quantum confinement effect, but more possible related to the surface or defect states and charge carrier delocalization in $MAPbI_3$[20]. For the samples from P-I1Br1-2 to P-I1Br1-5, the lifetime τ_{ave} boosts from 1.1 to 42.1 ns. While for the samples from P-Br-2 to P-Br-5, the lifetime τ_{ave} only increases from 13.0 to 17.1 ns, with the small PL peak shift from 532 to 525 nm. Compared with $MAPbBr_3$ single crystal or film (Table 2), these as prepared $MAPbBr_3$ nanocrystals exhibit shorter lifetime, suggesting more nonradiative recombination effect involved[13,56,57]. Unfortunately, there was no lifetime data of $MAPbBr_xI_{3-x}(0 \leq x \leq 3)$ quantum dots synthesized by using ammonium cation with a long alkyl chain as surface capping ligands[35–39]. Further investigation on how surface ligands type would affect the fluorescence lifetime may give us a deeper understanding of the exciton recombination dynamics, and thus better control of the PL for future use in construction of devices.

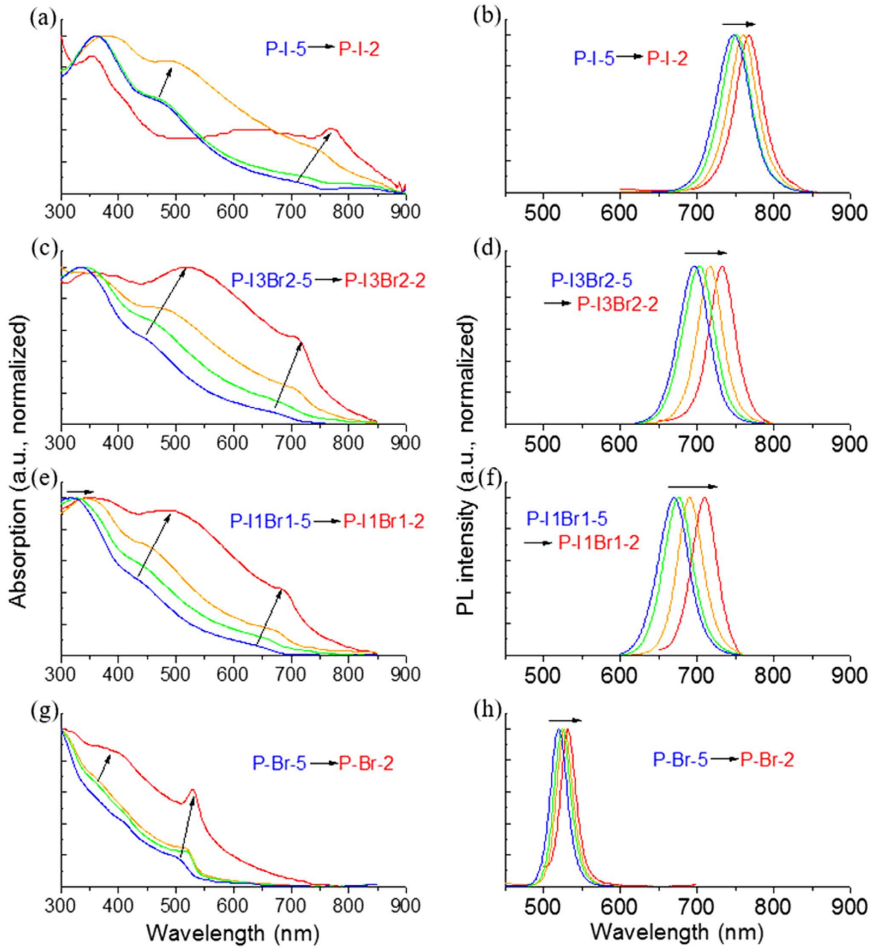

Figure 5. The UV-vis absorption spectra and PL spectra of four sets of samples: (**a**,**b**) P-I-2/3/4/5, (**c**,**d**) P-I3Br2-2/3/4/5, (**e**,**f**) P-I1Br1-2/3/4/5, and (**g**,**h**) P-Br-2/3/4/5. The arrows indicate the spectrum evolution of the samples (Excitation: 365 nm).

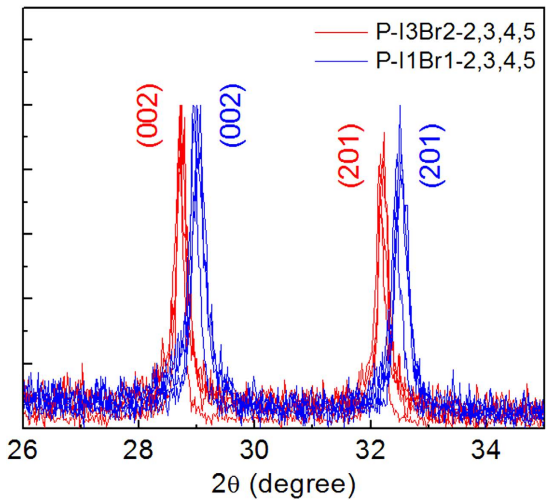

Figure 6. The XRD peaks of (002) and (201) for P-I3Br2-2/3/4/5 and P-I1Br1-2/3/4/5.

Conclusions

Organometal halide perovskite $MAPbBr_xI_{3-x}(0 \leq x \leq 3)$ colloidal nanocrystals were synthesized by mixing $Pb(OA)_2$ cyclohexane solution and MAX(X = I or/and Br) isopropanol solution. The size of the perovskites was

Sample	τ_1 (ns)	τ_2 (ns)	τ_{av} (ns)	PL λ_{Peak} (nm)
P-I-2	1.2	4.8	3.0	768
P-I-3	2.7	34.3	18.3	760
P-I-4	3.5	87.3	66.8	752
P-I-5	25.5	201. 7	166.2	748
P-I1Br1-2	0.47	4.1	1.1	710
P-I1Br1-3	0.46	15.1	10.6	690
P-I1Br1-4	5.0	47.0	35.9	676
P-I1Br1-5	6.8	55.6	42.1	670
P-Br-2	0.85	16.8	13.0	532
P-Br-3	2.9	24.5	16.9	527
P-Br-4	2.8	25.2	17.0	526
P-Br-5	3.0	24.1	17.1	525

Table 1. The fitting decay lifetimes of τ_1 and τ_2, the average lifetime τ_{ave} and corresponding PL peak.

Material	Size/shape/form	Lifetime (ns)	PL λ_{Peak} (nm)	Phase
$MAPbI_3$	bulk[26]	30	775	T
	nanowires ($d = 100$ nm)[26]	45	765	T
	film (800 nm)[58]	80	774	T
	bulk $0.3 \times 2\,\mu m$[34]	9	762	T
	wires 1500×34 nm[34]	30	756	T
	rods 810×54 nm[34]	66	760	T
	film[59]	9.6	~770	—
	films ($20\,\mu m^2$)[60]	~5	~751	—
$MAPbBr_3$	single crystal[61]	41, 57	570	C
	film[61]	13, 168	560	C
	film[62]	100	530	C
	nanocrystal 3.3 nm[36]	13.5	515	C

Table 2. Reported decay lifetimes and corresponding PL peaks for $MAPbI_3$ and $MAPbBr_3$, T = tetragonal, C = cubic.

successfully controlled by the oleate as the ligands, and also by the Pb:MA ratio. The UV-vis absorption and PL spectra show a blue shift as the size decreasing monotonically, which is ascribed for quantum confinement effect. Significantly, these colloidal organometal halide perovskite nanocrystals were dispersed well in nonpolar organic solvent, e.g. toluene or cyclohexane. This would be useful for fabricating perovskite thin films in various substrates such as silicon, polymer or glass. In addition to the method could be generally applied to synthesize other organometal halide perovskite materials, this study would bring chances to the design and fabrication of new photovoltaic and electronic devices.

Materials and Methods

Materials. Lead acetate trihydrate (AR), sodium oleate (>99.5%) and cyclohexane (>99.5%) were bought from Sinopharm. Isopropanol (anhydrous, 99.5%) was purchased from J&K. Hydroiodic acid (HI, 55–58%), hydrobromic acid (HBr, 47.0%) were purchased from Sigma-Aldrich. Methylamine (40% in methanol) was bought from TCI. All chemicals were used as received unless specified otherwise.

Synthesis of $Pb(OA)_2$ (OA = Oleic acid). The lead acetate solution (1.037 g in 5 mL H_2O) was added into the solution of sodium oleate (1.90 g in 25 mL mixture of ethanol and H_2O v:v = 1:1) with vigorous stirring. The precipitate ($Pb(OA)_2$) was separated by centrifugation, washed with water and finally dried in oven at 85 °C overnight.

Synthesis of MAX (MA = methylammonium, X = I, Br). Hydroiodic acid (10 mL, 0.075 mol) or hydrobromic acid (8.6 mL, 0.075 mol) was added to a solution of excess methylamine (24 mL, 0.192 mol) dropwisely at 0 °C under stirring. The mixture was continuously stirred in the ice bath for 2 hrs. The raw product (MAI or MABr) was obtained after evaporation and dried under dynamic vacuum at 60 °C for 12 hrs. The purified MAI or MABr was obtained by recrystallization from a mixed solvent of diethyl ether and ethanol.

Synthesis of $MAPbBr_xI_{3-x}$ ($0 \leq x \leq 3$) nanocrystals. Typically, $Pb(OA)_2$ (15.4 mg, 0.02 mmol) was dissolved in cyclohexane (20 mL) to form a solution A. MAI (6.4 mg, 0.04 mmol) was dissolved in isopropanol (20 mL) to make a solution B. Solution A was injected into to solution B with volume ratio of 1:1. The perovskite

$MAPbI_3$ nanocrystals can be isolated by centrifugation (3 min at 14000 rpm) and redispersed in solvent of cyclohexane or toluene. The $MAPbBr_xI_{3-x}(0 \leq x \leq 3)$ nanocrystals was synthesized similarly, by introducing MABr to the reaction. The samples are numbered in the form of P-I-*y*, P-I*a*Br*b*-*y*, or P-Br-*y*, where P = perovskite; *a* and *b* are the I:Br ratio of *a*:*b* such as I1Br1 or I2Br3; *y* = 2, 3, 4 or 5 means the MA:Pb ratio of y:1 (Table S1). "P-I-2/3/4/5" means four samples of different *y* values: P-I-2, P-I-3, P-I-4 and P-I-5. To eliminate the effects from the solvent, the volume ratio of cyclohexane to isopropanol is controlled as a constant of 1:1 for all the reactions in the context. The $Pb(OA)_2$ is kept as a constant. The concentration of MA in isopropanol is investigated as a variable.

Instruments. The powder X-ray Diffraction (XRD) spectra were performed on a Bruker D8 Advance instrument with a Cu Kα radiation (λ = 1.5418 Å). The scanning electron microscopy (SEM) images were obtained on the S-4800 SEM at 20 kV. The transmission electron microscopy (TEM) images were measured on a HT7700 (Hitachi) TEM at an acceleration voltage of 100 kV. The FTIR spectra were recorded on a Vector 22 spectrometer with a resolution of 2 cm^{-1} by using KBr pellets. The absorption spectra were obtained by a Shimadzu UV-2700 UV/Vis spectrophotometer. The PL spectra were collected with a Hitachi F-4600 fluorescence spectrophotometer. PL lifetimes were measured with a Zolix Omini-λ 300 fluorescence spectrophotometer and a picosecond pulsed diode laser (Edinburgh Instruments Ltd.) operating at 379.2 nm.

References

1. Kojima, A., Teshima, K., Shirai, Y. & Miyasaka, T. Organometal Halide Perovskites as Visible-Light Sensitizers for Photovoltaic Cells. *J. Am. Chem. Soc.* **131,** 6050–6051 (2009).
2. Kim, H. S., Im, S. H. & Park, N. G. Organolead Halide Perovskite: New Horizons in Solar Cell Research. *J. Phys. Chem. C* **118,** 5615–5625 (2014).
3. Lee, M. M., Teuscher, J., Miyasaka, T., Murakami, T. N. & Snaith, H. J. Efficient Hybrid Solar Cells Based on Meso-Superstructured Organometal Halide Perovskites. *Science* **338,** 643–647 (2012).
4. Burschka, J. *et al.* Sequential Deposition as a Route to High-Performance Perovskite-Sensitized Solar Cells. *Nature* **499,** 316–319 (2013).
5. Green M. A., Ho-Baillie A. & Snaith H. J. The Emergence of Perovskite Solar Cells. *Nat. Photonics* **8,** 506–514 (2014).
6. Jeon, N. J. *et al.* Solvent Engineering for High-Performance Inorganic–Organic Hybrid Perovskite Solar Cells. *Nat. Mater.* **13,** 897–903 (2014).
7. Zhou, H. *et al.* Interface Engineering of Highly Efficient Perovskite Solar Cells. *Science* **345,** 542–546 (2014).
8. Jeon, N. J. *et al.* Compositional Engineering of Perovskite Materials for High-Performance Solar Cells. *Nature* **517,** 476–480 (2015).
9. Li, X. *et al.* A vacuum flash–assisted solution process for high-efficiency large-area perovskite solar cells. *Science* **353(6294),** 58–62 (2016).
10. Tan, Z. K. *et al.* Bright Light-Emitting Diodes Based on Organometal Halide Perovskite. *Nat. Nanotechnol.* **9,** 687−692 (2014).
11. Li, G. *et al.* Efficient Light-Emitting Diodes Based on Nanocrystalline Perovskite in a Dielectric Polymer Matrix. *Nano Lett.* **15,** 2640−2644 (2015).
12. Song, J. *et al.* Quantum Dot Light-Emitting Diodes Based on Inorganic Perovskite Cesium Lead Halides ($CsPbX_3$). *Adv Mater.* **27,** 7162–7167 (2015).
13. Yantara, N. *et al.* Inorganic Halide Perovskites for Efficient Light-Emitting Diodes. *J. Phys. Chem. Lett.* **6,** 4360–4364 (2015).
14. Kumawat, N. K. *et al.* Band Gap Tuning of $CH_3NH_3Pb(Br_{1-x}Cl_x)_3$ Hybrid Perovskite for Blue Electroluminescence. *ACS Appl. Mater. Inter.* **7,** 13119–13124 (2015).
15. Ling, Y. *et al.* Bright Light-Emitting Diodes Based on Organometal Halide Perovskite Nanoplatelets. *Adv. Mater.* **28,** 305–311 (2016).
16. Aharon, S. & Etgar, L. Two Dimensional Organometal Halide Perovskite Nanorods with Tunable Optical Properties. *Nano Lett.* **16,** 3230–3235 (2016).
17. Täuber, D., Dobrovolsky, A., Camacho, R. & Scheblykin, I. G. Exploring the Electronic Band Structure of Organometal Halide Perovskite via Photoluminescence Anisotropy of Individual Nanocrystals. *Nano Lett.* **16,** 5087–5094 (2016).
18. Xing, G. *et al.* Low-Temperature Solution-Processed Wavelength-tunable Perovskites for Lasing. *Nat. Mater.* **13,** 476–480 (2014).
19. Dhanker, R. *et al.* Random Lasing in Organo-Lead Halide Perovskite Microcrystal Networks. *Appl. Phys. Lett.* **105,** 151112 (2014).
20. Protesescu, L. *et al.* Nanocrystals of Cesium Lead Halide Perovskites ($CsPbX_3$, X = Cl, Br, and I): Novel Optoelectronic Materials Showing Bright Emission with Wide Color Gamut. *Nano Lett.* 15, 3692−3696 (2015).
21. Nedelcu, G. *et al.* Fast Anion-Exchange in Highly Luminescent Nanocrystals of Cesium Lead Halide Perovskites ($CsPbX_3$, X = Cl, Br, I). *Nano Lett.* **15,** 5635–5640 (2015).
22. Zhang, D., Eaton, S. W., Yu, Y., Dou, L. & Yang, P. Solution-Phase Synthesis of Cesium Lead Halide Perovskite Nanowires. *J. Am. Chem. Soc.* **137,** 9230–9233 (2015).
23. Akkerman, Q. A. *et al.* Tuning the Optical Properties of Cesium Lead Halide Perovskite Nanocrystals by Anion Exchange Reactions. *J. Am. Chem. Soc.* **137,** 10276–10281 (2015).
24. Fu, Y. *et al.* Solution Growth of Single Crystal Methylammonium Lead Halide Perovskite Nanostructures for Optoelectronic and Photovoltaic Applications. *J. Am. Chem. Soc.* **137,** 5810−5818 (2015).
25. Horváth, E. *et al.* Nanowires of Methylammonium Lead Iodide ($CH_3NH_3PbI_3$) Prepared by Low Temperature Solution-Mediated Crystallization. *Nano Lett.* **14,** 6761–6766 (2014).
26. Im, J. H. *et al.* Nanowire Perovskite Solar Cell. *Nano Lett.* **15,** 2120–2126 (2015).
27. Zhao, Y. *et al.* Improving the Efficiency of Perovskite Solar Cells through Optimization of the $CH_3NH_3PbI_3$ Film Growth in Solution Process Method. *Appl. Surf. Sci.* **359,** 560–566 (2015).
28. Moore, D. T. *et al.* Crystallization Kinetics of Organic–Inorganic Trihalide Perovskites and the Role of the Lead Anion in Crystal Growth. *J. Am. Chem. Soc.* **137,** 2350–2358 (2015).
29. Ramirez, D., Escobar, M. A. M., Montoya, J. F. & Jaramillo, F. Understanding the Role of the Mesoporous Layer in the Thermal Crystallization of a Meso-Superstructured Perovskite Solar Cell. *J. Phys. Chem. C* **120,** 8559–8567 (2016).
30. Chung, C. C., Lee, C. S., Jokar, E., Kim, J. H. & Diau E. W. G. Well-Organized Mesoporous TiO_2 Photoanode by Using Amphiphilic Graft Copolymer for Efficient Perovskite Solar Cells. *J. Phys. Chem. C* **120,** 9619–9627 (2016).
31. Son, D. Y., Im, J. H., Kim, H. S. & Park, N. G. 11% Efficient Perovskite Solar Cell Based on ZnO Nanorods: An Effective Charge Collection System. *J. Phys. Chem. C* **118,** 16567–16573 (2014).
32. Schmidt, L. C. *et al.* Nontemplate Synthesis of $CH_3NH_3PbBr_3$ Perovskite Nanoparticles. *J. Am. Chem. Soc.* **136,** 850−853 (2014).
33. Tyagi, P., Arveson, S. M. & Tisdale, W. A. Colloidal Organohalide Perovskite Nanoplatelets Exhibiting Quantum Confinement. *J. Phys. Chem. Lett.* **6,** 1911–1916 (2015).
34. Zhu, F. *et al.* Shape Evolution and Single Particle Luminescence of Organometal Halide Perovskite Nanocrystals. *ACS Nano* **9,** 2948–2959 (2015).

35. Sichert, J. A. *et al.* Quantum Size Effect in Organometal Halide Perovskite Nanoplatelets. *Nano Lett.* **15,** 6521–6527 (2015).
36. Zhang, F. *et al.* Brightly Luminescent and Color-Tunable Colloidal $CH_3NH_3PbX_3$ (X = Br, I, Cl) Quantum Dots: Potential Alternatives for Display Technology. *ACS nano* **9,** 4533–4542 (2015).
37. Liang, K. N., Mitzi, D. B. & Prikas, M. T. Synthesis and Characterization of Organic−Inorganic Perovskite Thin Films Prepared Using a Versatile Two-Step Dipping Technique. *Chem. Mater.* **10,** 403–411 (1998).
38. Baikie, T. *et al.* Synthesis and Crystal Chemistry of the Hybrid Perovskite $(CH_3NH_3)PbI_3$ for Solid-State Sensitised Solar Cell Applications. *J. Mater. Chem. A* **1,** 5628–5641 (2013).
39. Stoumpos, C. C., Malliakas, C. D. & Kanatzidis, M. G. Semiconducting Tin and Lead Iodide Perovskites with Organic Cations: Phase Transitions, High Mobilities, and Near-Infrared Photoluminescent Properties. *Inorg. Chem.* **52,** 9019–9038 (2013).
40. Kawamura, Y., Mashiyama, H. & Hasebe, K. Structural Study on Cubic-tetragonal Transition of $CH_3NH_3PbI_3$. *J. Phys. Soc. Jpn.* **71,** 1694–1697 (2002).
41. Kulkarni, S. A. *et al.* Band-Gap Tuning of Lead Halide Perovskites Using a Sequential Deposition Process. *J. Mater. Chem. A* **2,** 9221–9225 (2014).
42. Ahn, N. *et al.* Highly Reproducible Perovskite Solar Cells with Average Efficiency of 18.3% and Best Efficiency of 19.7% Fabricated via Lewis Base Adduct of Lead(II) Iodide. *J. Am. Chem. Soc.* **137,** 8696−8699 (2015).
43. Halder, A., Choudhury, D., Ghosh, S., Subbiah, A. S. & Sarkar, S. K. Exploring Thermochromic Behavior of Hydrated Hybrid Perovskites in Solar Cells. *J. Phys. Chem. Lett.* **6,** 3180−3184 (2015).
44. Xu, X. X., Zhuang, J. & Wang, X. SnO_2 Quantum Dots and Quantum Wires: Controllable Synthesis, Self-Assembled 2D Architectures, and Gas-Sensing Properties. *J. Am. Chem. Soc.* **130,** 12527–12535 (2008).
45. Wang, G. *et al.* Colloidal Nanocrystals Fluoresced by Surface Coordination Complexes. *Sci. Rep.* **4,** 5480 (2014).
46. Lide, D. *CRC Handbook of Chemistry and Physics*, 73rd edition. CRC Press (1993).
47. Koutselas, I. B., Ducasse, L. & Papavassiliou, G. C. Electronic Properties of Three-and Low-Dimensional Semiconducting Materials with Pb Halide and Sn Halide Units. *J. Phys.: Condens. Matter* **8,** 1217 (1996).
48. Hirasawa, M., Ishihara, T., Goto, T., Uchida, K. & Miura, N. Magnetoabsorption of the Lowest Exciton in Perovskite-Type Compound $(CH_3NH_3)PbI_3$. *Physics B* **201,** 427–430 (1994).
49. Tanaka, K. *et al.* Comparative Study on the Excitons in Lead-Halide-Based Perovskite Type Crystals $CH_3NH_3PbBr_3$ $CH_3NH_3PbI_3$. *Solid State Commun.* **127,** 619–623 (2003).
50. Fisher, B. R., Eisler, H. J., Stott, N. E. & Bawendi, M. G. Emission Intensity Dependence and Single-Exponential Behavior in Single Colloidal Quantum Dot Fluorescence Lifetimes. *J. Phys. Chem. B* **108,** 143–148 (2004).
51. Tang, J. *et al.* Colloidal-Quantum-Dot Photovoltaics Using Atomic-Ligand Passivation. *Nat. Mater.* **10,** 765–771 (2011).
52. He, H. *et al.* Exciton localization in solution-processed organolead trihalide perovskites. *Nat. Commun.* **7,** 10896 (2016).
53. Park, J. *et al.* Ultra-large-scale syntheses of monodisperse nanocrystals. *Nat. Mater.* **3,** 891–895 (2014).
54. Hendricks, M. P., Campos, M. P., Cleveland, G. T., Plante, I. J. L. & Owen, J. S. A tunable library of substituted thiourea precursors to metal sulfide nanocrystals. *Science* **348,** 1226–1230 (2015).
55. Mokari, T., Habas, S. E. & Zhang, M. Synthesis of lead chalcogenide alloy and core–shell nanowires. *Angew. Chem. Int. Ed* **47,** 5605–5608 (2008).
56. D'Innocenzo, V., Kandada, A. R. S., Bastiani, M. D., Gandini, M. & Petrozza, A. Tuning the Light Emission Properties by Band Gap Engineering in Hybrid Lead Halide Perovskite. *J. Am. Chem. Soc.* **136,** 17730–17733 (2014).
57. Yang, Y. *et al.* Comparison of Recombination Dynamics in $CH_3NH_3PbBr_3$ and $CH_3NH_3PbI_3$ Perovskite Films: Influence of Exciton Binding Energy. *J. Phys. Chem. Lett.* **6,** 4688–4692 (2015).
58. Saba, M. *et al.* Correlated electron-hole plasma in organometal perovskites. *Nat. Commun.* **5,** 5049 (2014).
59. Stranks, S. D. *et al.* Electron-Hole Diffusion Lengths Exceeding 1 Micrometer in an Organometal Trihalide Perovskite Absorber. *Science* **342,** 341–344 (2013).
60. Nie, W. Y. *et al.* High-Efficiency Solution-Processed Perovskite Solar Cells with Millimeter-Scale Grains. *Science* **347,** 522–525 (2015).
61. Shi, D. *et al.* Low Trap-State Density and Long Carrier Diffusion in Organolead Trihalide Perovskite Single Crystals. *Science* **347,** 519–522 (2015).
62. Zhang, M. *et al.* Composition-Dependent Photoluminescence Intensity and Prolonged Recombination Lifetime of Perovskite $CH_3NH_3PbBr_{3-x}Cl_x$ films. *Chem. Commun.* **50,** 11727–11730 (2014).

Acknowledgements

This work was supported by the Major State Basic Research Development Program of China (Grant No. 2013CB922102), the project of Scientific and Technological Support Program in Jiangsu province (BE2014147-2), the National Natural Science Foundation of China (Grant No. 51572120, 21271099, 21301089) and Jiangsu Province Science Foundation for Youths (BK20130562).

Author Contributions

X.X. conceived the experiments. Y.Z. conducted the experiments. All authors contributed to the results analysis, discussion and drafting of the manuscript.

Additional Information

Supplementary information accompanies this paper at http://www.nature.com/srep

Competing financial interests: The authors declare no competing financial interests.

How to cite this article: Zhao, Y. *et al.* Colloidal Organometal Halide Perovskite ($MAPbBr_xI_{3-x}$, $0 \le x \le 3$) Quantum Dots: Controllable Synthesis and Tunable Photoluminescence. *Sci. Rep.* **6**, 35931; doi: 10.1038/srep35931 (2016).